BULLETIN OF THE POLISH ACADEMY OF SCIENCES
TECHNICAL SCIENCES
DOI: 10.24425/bpasts.2024.149815

Piezoresistive response of geopolymer pastes activated by silica fume-derived alkaline solution

Murugan Muthu* and Łukasz Sadowski

Department of Materials Engineering and Building Processes, Wroclaw University of Science and Technology,
Wybrzeże Wyspiańskiego 27, 50-372 Wrocław, Poland

Abstract. This study examined the self-sensing performance of metakaolin-based geopolymer paste samples activated by an alkali activator, which is a solution mixture of potassium hydroxide and silica fume (SF). Their piezoresistive response under repeated compressive loads was found to improve with increasing SF content. It was found from their XRD, SEM, and FTIR results that the change in the SF content did not alter the phase composition of the geopolymer matrices. The factorial change in the electrical resistivity of geopolymer samples with a maximum SF content was calculated to be about 0.024. Their pore solutions were detected to be mainly filled with potassium and silicon ions due to the use of higher concentrations of SF particles. The UV spectrophotometry measurements of this study confirm that all the geopolymer samples displayed semiconductor behaviour. The SF-derived alkaline activator can enable the self-sensing character of geopolymer-based concrete, which is environmentally friendly and has recently shown great potential to monitor structural integrity under applied external loads.

Key words: geopolymer; metakaolin; silica fume; alkaline activator; piezoresistivity; microstructure

1. INTRODUCTION

Structural concrete is often used to build tunnels, ports, bridges, and nuclear power plants. Ageing and deterioration of concrete during its service life will lead to loss of structural integrity and, therefore, it is necessary to monitor the structural state to ensure the safety [1]. Conventional sensors are embedded in steel reinforced concrete to monitor their internal condition, but they have their own disadvantages, including high cost, insufficient durability, and compatibility problems with deformed structural materials [2]. Research has been demonstrated to enable the self-sensing potential in concrete [3]. The main result of the research is the infusion of functional fillers that form an extensive conductive path within the matrix [4]. To date, conductive fillers that have been popularly reviewed are carbon nanomaterials, steel fibre, and graphite [5]. Nanomaterials have a large surface area and outstanding properties [6], and their infusion into cement mixes showed mostly promising results [7]. However, to achieve their uniform dispersion within the cement matrix is very costly and time consuming.

Geopolymer (GP), a cement-free binder, is synthesized by mixing alkali activators with aluminosilicate materials [8]. Common activators are mixtures of the Na_2SiO_3-NaOH and K_2O_3Si-KOH solution [9], while the most successful precursors used in the synthesis of GP are fly ash, slag, calcined clay, volcanic ash and metakaolin [10]. The GP matrix exhibits a reasonably high electrolytic conductivity because of the free metallic ions available in its matrix. It has many advantages over cement, including reducing greenhouse gas emissions during production, improving acid resistance, and higher initial compressive strength. The GP conductivity range was found to be 10^{-6} to 10^{-3} S/cm [11], allowing it to be used as sensors for concrete strain, temperature, and moisture. The GP mix was demonstrated to possess a direct piezoelectric effect originating from the migration of mobile hydrated cations into the pores of the cross-linked aluminosilicate structure under applied external loads [12]. The addition of graphene oxide at 0.35% by weight increased the electrical conductivity of GP based on fly ash by 209% [13]. Saafi et al. [14] used carbon nanotubes (CNT) up to 0.5 by weight to improve the self-sensing potential of the fly ash-based GP mix. Bi et al. [15] dispersed 0.25% SiO_2 coated CNT by volume in the metakaolin-based GP mix to improve the sample conductivity. This SiO_2 coating improved the CNT dispersion in the GP mix.

McAlorum et al. [9] spray coated the self-sensing GP mix on the concrete substrate robotically to monitor temperature and deformation in real time. The pore solution of the GP binder strongly influences its intrinsic behaviour. It is composed of alkali and metal cations (i.e., Na^+, K^+, Al^{3+}, Si^{4+}, Ca^{2+}, and Mg^{2+}). The alkaline activator dissolves the chemical species of precursor, followed by orientation, polycondensation, and formation of a three-dimensional (3D) tetrahedral AlO_4^--SiO_4

*e-mail: murugan.muthu@pwr.edu.pl

framework [16]. Cross-linking of SiO_4 and AlO_4 tetrahedra is bound by sharing oxygen atoms, while the negative charge of Al^{3+} ions in four-fold coordination is balanced with alkalis (either Na^+ or K^+). The type and composition of raw materials influences the structure of such a 3D network [17], which can be amorphous, semicrystalline, or crystalline. Cai et al. [18] found that the thermoelectric property of fly ash-based and metakaolin-based GP mixes improved with an increasing concentration of alkalis in their pore solutions. Addition of fly ash reduces capillary porosity and hydroxyl ions, resulting in decreased permeability and increased electrical resistance [19]. Previous research on GP samples investigated the effect of its precursor type on the self-sensing character [20]. Geopolymerization between silica fume and aluminum ions during processing has been reported to lead to the formation of strong interconnections between the starting particles, resulting in an increase in the mechanical strength of the hardened matrix [21]. The use of metakaolin showed improved conductivity because the raw material is processed in a controlled environment unlike industrial by products (i.e., fly ash and slag) and exhibits constant chemical characteristics [22]. However, the composition of the alkaline activator used also influences such an intrinsic property, which is typically described as the K_2O(or Na_2O)/SiO_2 ratio. This composition parameter determines the number of bridging oxygens and the proportion of siloxo to di-siloxomers within the tetrahedral AlO_4^--SiO_4 framework (i.e., GP structure).

To fill this research gap, a metakaolin-based geopolymer paste sample that was activated by an alkaline activator based on silica fume and potassium hydroxide was prepared. The effects of such activating materials on the self-sensing properties of the GP mixes were examined by obtaining its piezoresistive response under cyclic compression load, which was maintained well below the elastic regime of the sample until the end of the test. The heat, strength, and conductivity developments of such GP mixes with time were also found using isothermal calorimetry, compressive strength machine, and digital multimeter with 0.0035% accuracy. The microstructural properties of such mixes at the end of 28 days were also determined by performing X-ray diffraction (XRD), Fourier transform infrared spectroscopy (FTIR), scanning electron microscopy (SEM) and ultraviolet visible spectrophotometry (UV-Vis) studies. The pore solution was extracted from these GP mixes at the end of 28 days using an extraction device equipped with an air circulator, and the concentration of alkali and metal cations remaining in such a solution was determined by inductively coupled plasma optical emission spectroscopy (ICP-OES). The pH of such a solution was also monitored. With these experimental investigations, the optimal composition of the SF-derived alkali activator was examined to elucidate the self-sensing potential of the GP mix and the effect of the composition of such an alkali activator on the hydration, electrical, mechanical, and microstructural properties of the GP binder that can be used in structural health monitoring applications was also discussed.

2. EXPERIMENTAL PROGRAM

2.1. Raw materials

The GP paste mixes were made using metakaolin, silica fume, potassium hydroxide, and distilled water. High-purity metakaolin (MK) was obtained from BASF, while silica fume (SF) and potassium hydroxide (KOH) pellets were obtained from Cabot Cooperation and Merck. High purity, analytical grade KOH pellets were used. The MK and SF particles were ground to a size of less than 45 µm using a standard sieve and then scanned using a Bruker D8 model XRD with a source of Cu Kα source, operating at a current of 40 mA and a voltage of 40 kV, respectively. These samples were scanned at a rate of 0.02°/min for a diffraction angle (2θ) range of 5-80°. Fig. 1 shows their XRD results. The quartz compound (SiO_2) was observed mainly in SF, while MK was composed of mullite ($3Al_2O_3{\cdot}2SiO_2$) and anatase (TiO_2) traces. The chemical composition of MK and SF was determined using Rigaku Nex-CG X-ray fluorescence (XRF). A semiautomatic pelletiser was used to compact the powder samples in a circular metal plate, and then XRF analyses were performed. Table 1 lists the XRF results. The loss of ignition of both SF and MK was found to be low, indicating that these materials do not contain carbon species and organic matter in them.

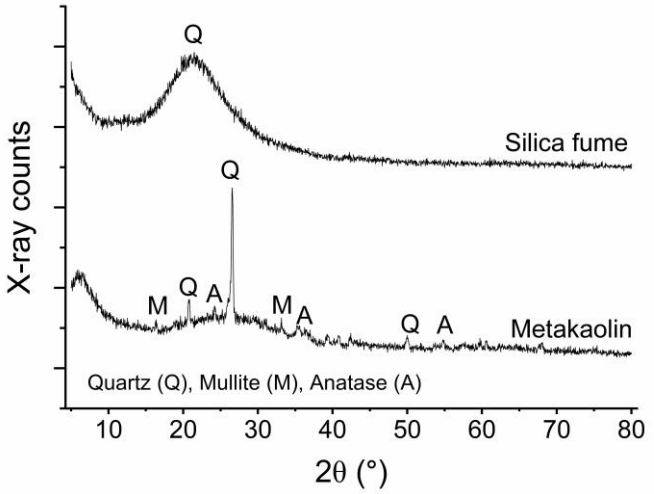

Fig. 1 XRD pattern of silica fume and metakaolin

Table 1 Chemical composition of raw materials

Oxide Compounds	Metakaolin	Silica fume
Calcium oxide, CaO %	0.02	0.11
Silicon dioxide, SiO_2 %	53.11	94.22
Aluminium oxide, Al_2O_3 %	43.87	0.76
Iron oxide, Fe_2O_3 %	0.43	0.25
Magnesium oxide, MgO %	0.03	0.51
Sulfur trioxide, SO_3 %	0.03	0.36
Sodium oxide, Na_2O %	0.23	0.25
Potassium oxide, K_2O %	0.19	0.98
Titanium dioxide, TiO_2 %	1.71	-
Loss in ignition %	0.38	2.56

2.2. Sample preparation

Three GP paste mixes were prepared with 750 g of MK, but were made with varying amounts of alkaline activators, including 1758, 1806, and 1855 g, respectively. The ratio of precursor-to-alkaline activator by weight of these mixes was calculated to be 0.43, 0.41, and 0.4. The quantity of metakaolin (i.e., precursor) was kept constant in such mixes, but the composition of alkaline activators was altered to understand their effects on the sensing potential of GP mixes. Such combinations were designed based on trial and error. Table 2 lists the composition of different alkaline activators. The KOH pellets were dissolved in an SF-water mixture with the help of a laboratory magnetic stirrer as illustrated in Fig. 2. Care was taken to avoid an increase in the solution temperature above 40 °C. The final solution mixture was observed to be colourless after the complete dissolution of the KOH pellets. The mixture was cooled overnight at room temperature. MK and this alkaline solution were mixed in a Kenwood model stand mixer for five minutes and poured into acrylic moulds of different sizes. Mild vibration was applied to consolidate these fresh samples using a vibration table, and their top surfaces were smooth finished using a tapping knife. The upper surface of the fresh samples was covered with a thin polyethylene wrap to prevent moisture loss. After 24 hours, the samples were demolded and cured in a moist environment at 25 °C and 65% relative humidity (RH) until the age of the test.

Table 2 Composition of alkaline activators used in the preparation of geopolymer samples

Sample name	Silica fume (g)	Potassium hydroxide (g)	Water (g)
GP1	280	434	1044
GP2	328	434	1044
GP3	377	434	1044

2.3. Test methods

2.3.1. Isothermal calorimetry

This test was carried out at 25 °C and 65% RH according to ASTM C1702 [23]. The fresh paste sample of a 30 g quantity was loaded into the test channel of an I-Cal 8000 Calmetrix high precision isothermal calorimeter. The heat developments in such a sample were recorded for up to 72 hours.

2.3.2. Compressive strength test

The cubic paste sample of size 50 × 50 × 50 mm^3 was crushed in a Toni Technik compression test machine at a load rate of 100 kN/min. This test was carried out according to ASTM C109 [24]. The load at failure was divided with the cross-sectional area of the sample to calculate the strength value. The average of four replicates was determined.

2.3.3. Electrical conductivity test

This test method works according to the Wenner four-point principle. We adopted the same procedure as recommended by Ma et al. [25]. A paste sample of size 12.5 × 12.5 × 75 mm^3 was cast, cured in air and copper adhesive was bound to its exterior surfaces at designated intervals, which is shown in Fig. 3 schematically. An electric current of 50 µA was applied to this dry sample using a Keithley 6221 model AC source. Meanwhile, voltage was recorded using a GW Instek GDM-8261A model digital multimeter with 0.0035% accuracy. During this experiment, a high frequency of 1 kHz was maintained to reduce the polarization effects. After 10 minutes, the sample conductivity readings were recorded. The average of three replicates were calculated.

2.3.4. Piezoresistivity test

This electromechanical test was conducted on a cubic paste sample sized 50 × 50 × 50 mm^3. Fig. 4 schematically explains this test arrangement. Two numbers of 1 mm thick gauze steel mesh were embedded in this sample at equidistant locations to determine the piezoresistivity of the sample under applied external loads. The size of a single grid in each mesh is approximately 2.5 × 2.5 mm^2. During casting, the bottom mesh was placed on top of the first layer of fresh paste filled in the mould, and then the top mesh was embedded over the second layer of paste sample. Care was taken to prevent the movement of the mesh during the consolidation of the fresh sample. A constant compression loading of 10 kN was applied to this specially prepared specimen using an MTS servo-hydraulic test machine with a maximum capacity of 250 kN. Five loading cycles were maintained to collect enough information on changes in electrical resistance at a rate of 12.5 kN/min. A multimeter was used to record changes in electrical resistance.

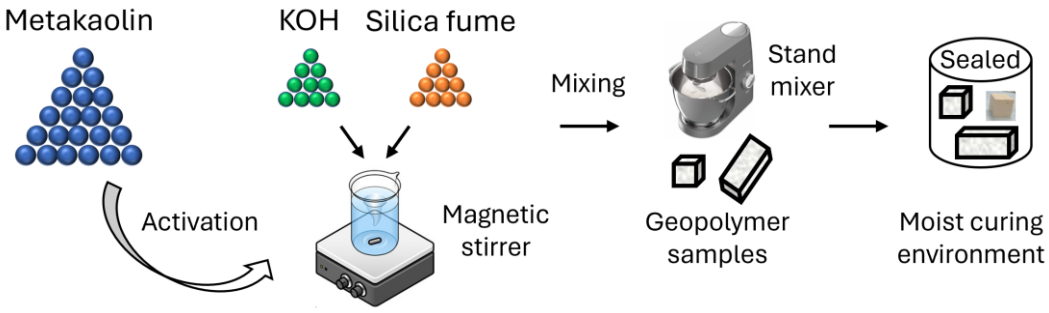

Fig. 2 Mixing process of geopolymer samples

2.3.5.Pore solution extraction

A paste sample of 8 mm in diameter and 26 mm in length was cast and cured in moist air for up to 72 hours. This sample was loaded into a high-pressure extraction device, as illustrated in Fig. 5. A maximum load of 1200 kN was applied onto this sample-loaded extraction device at a rate of 1.2 kN/sec using an MTS compression test machine with a 3000 kN capacity. The CO_2 environment surrounding this test arrangement was filtered using an air circulator containing a NaOH solution of 1 mol/L equipped with the extraction device.

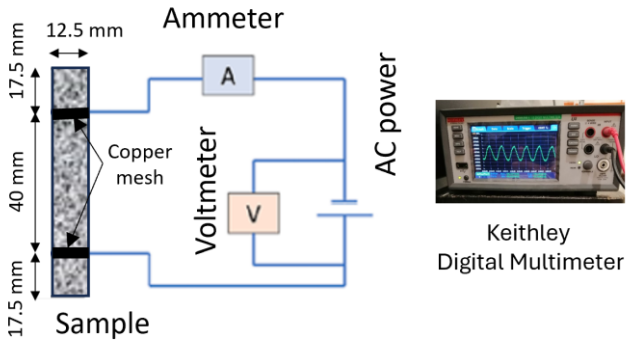

Fig. 3 Scheme of the electrical conductivity test

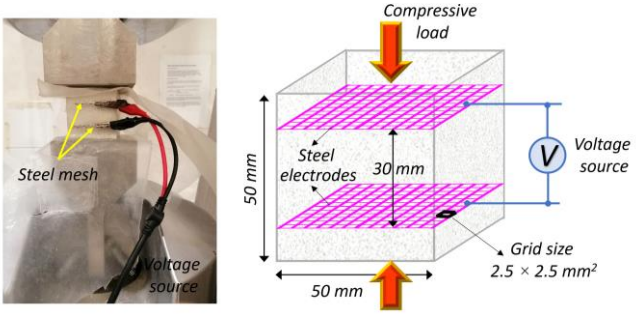

Fig. 4 Scheme of steel mesh embedded paste sample used in the piezoresistivity test

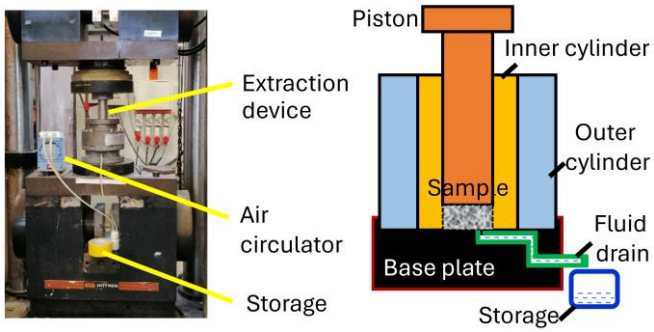

Fig. 5 Details of the pore solution extraction device

2.3.6.ICP-OES and pH meter

The extracted pore solution was filtered using 0.45 µm Whatman disk filters, diluted 1000 times, and then acidified with 2% HNO_3 to measure the concentration of Al^{3+}, Si^{4+}, and K^+ ions using a PerkinElmer Optima-8000 model ICP-OES instrument, which can detect such ions up to 0.01 µg/L concentration. The pH reading of this filtered solution was measured at 25 °C using a Horiba F-52 pH meter, which was calibrated by three points according to the NIST standards. The average of three readings was calculated.

2.3.7.FTIR, XRD, and UV-Vis spectroscopy

Geopolymer fragments obtained from compression tests performed after 28 days of mixing were powdered to a size smaller than 45 µm using a standard sieve. Laboratory mortar and pestle made of Agate rock were used to grind such samples. The powdered samples were then scanned in an XRD at a rate of 0.02° 2θ/min for 2θ range 5-80°. The mid-IR scans of such samples for a wavelength range 4000-400 cm^{-1} were obtained using a Thermo Scientific Nicolet-iS50 FTIR instrument. The UV-Vis spectrum of the synthesised GP sample was recorded at the end of 28 days on a PerkinElmer Lambda 950 spectrophotometer. Each spectrum was collected for a wavelength range of 200 to 800 nm with 64 transients at a resolution of 4 cm^{-1} in absorption mode at room temperature.

2.3.8.SEM

Geopolymer samples were cut into multiple pieces using a diamond-tipped precision saw. They were dried, epoxy impregnated using a Buehler Cast N'Vac 220 vacuum system and left undisturbed for 12 hours. This hardened epoxy polymer was polished on a metal disc at a speed of 300 rpm, followed by polishing again at 150 rpm using three different polycrystalline diamond sprays (of sizes 9, 3, and 1 µm). The Buehler Metaserv-250 model polishing machine was used. The fine polished surfaces were then imaged via a JEOL JSM-7600F equipment at a current of 20 kV under backscattered electron (BSE) mode. Carbon adhesive was used to mount the hardened epoxy polymer onto the metal stubs that were loaded into the SEM equipped with energy dispersive spectroscopy (EDS).

3. RESULTS AND DISCUSSION

3.1. Heat of hydration

Fig. 6 shows the calorimetry test results. All fresh mixes exhibited an exothermic reaction when the alkaline solution was mixed with MK. GP1, GP2 and GP3 exhibited maximum heat at 3.6, 5.3, and 6.3 hours after mixing. The total heat liberated by them at the end of 72 hours was calculated to be 534, 462, and 452 Joules per gram of the precursor used, respectively. The addition of more SF in the KOH solution not only reduced the heat evolved during the fresh GP hydration, but also delayed the setting time. The polymerisation mechanism of GP matrix is related to the dissolution-hydrolysis and hydrolysis-polycondensation processes [26]. Liang et al. [27] examined the hydration of fresh GP mixes prepared by activators with various silicate moduli. Heat developments increased in such GP mixes with a low silicate modulus as a result of the rapid dissolution of the soluble species and a much higher amount of formed reaction products. Li et al. [28] found that the GP mix experienced an initial chemical shrinkage, followed by an expansion and again a shrinkage during the hydration process. GP matrices with the structure of

poly(sialate), poly(sialate-disiloxo) and poly(sialate-multisiloxo) condense when their SiO_2/Al_2O_3 molar ratio is about 1-3 [29]. Mechanical [30] and durability [17] performance of GP mixes was found to be excellent when the SiO_2/Al_2O_3 ratio range varied between 3.5-4.5 [31].

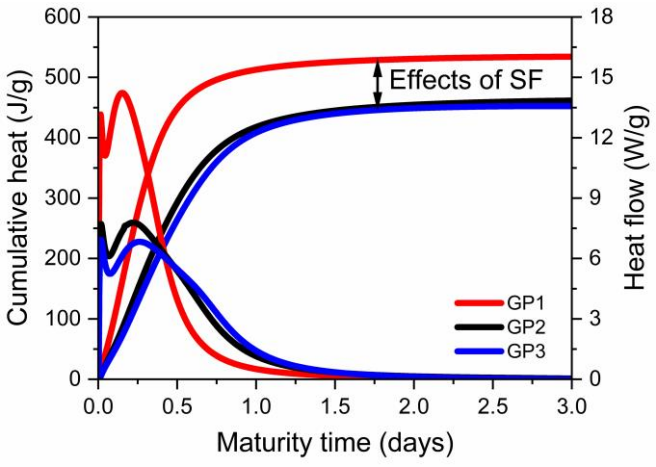

Fig. 6 Isothermal calorimetry test results

3.2. Compressive strength and electrical conductivity

Fig. 7 shows the compressive strength and electrical conductivity test results of the GP mixes. Their strength development over time was marginal, but its conductivity was found to reduce significantly with age. The mean strength of GP3 after 3, 7, 14, and 28 days was calculated to be 32, 33, 34, and 35 MPa. At the end of these days, the average conductivity of GP3 was 1.2, 0.9, 0.6, and 0.2 mS/cm, respectively. The GP conductivity was found to be inversely proportional to its strength. There is no significant change in the strength development after 3 days, indicating that the GP mixes reached the maximum strength within a few days after casting. GP3 at the end of 3 days was found to have the highest conductivity among the samples. The GP matrix is inherently brittle because its structure is a tetrahedral AlO_4^--SiO_4 framework [10]. In this study, the GP1 was made with a lower amount of SF and showed weak conductivity, regardless of age. The GP conductivity increased with increasing content of SF. The conductivity and strength of GP3 at the end of 28 days were calculated to be 21% and 49% higher than those of GP1. The amounts of SF in the KOH solution governed the performance of the GP pastes. Zhang et al. [32] found that the use of K-based alkaline solution improved the compressive strength of GP samples than the Na-based solution mixture. Bernal et al. [33] noticed similar reaction products in fly ash-slag blends activated by SF-derived alkaline activators and commercial silicate solutions because of the high reactivity of this precursor, which supplied high concentrations of Si^{4+} ions to systems since the early stages of the reaction. The GP sample activated by a SF-NaOH combination achieved 92% of the compressive strength of 28 days within 7 days of mixing, while this early age strength gain was 79% when the sample was synthesised using a commercial Na_2SiO_3-NaOH mixture [34].

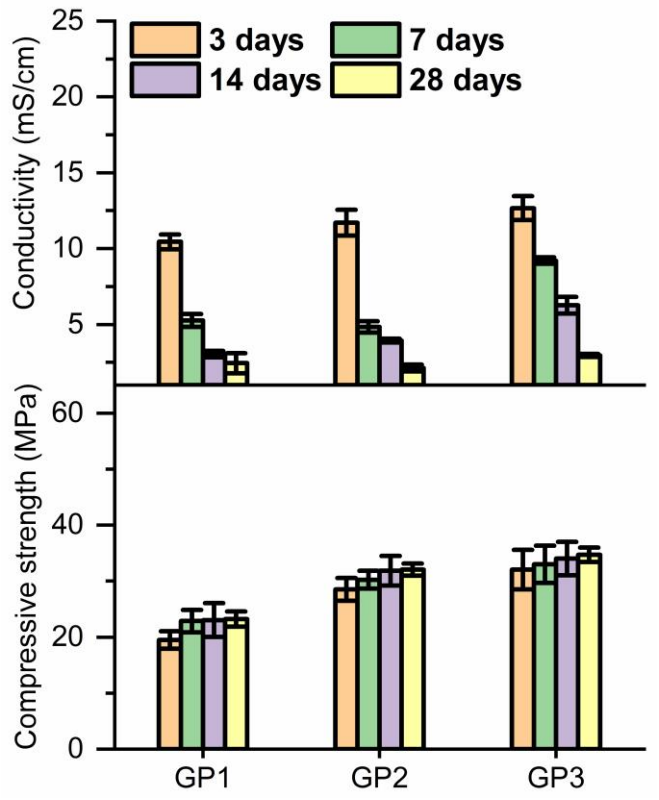

Fig. 7 Compressive strength and conductivity test results

3.3. Piezoresistive response under cyclic loading

Fig. 8 shows the results of the piezoresistivity test conducted on GP samples after 28 days of mixing. A maximum load of 10 kN was applied on such samples for five repetitive cycles. Care was taken to load these samples well below their elastic limit during the whole experiment. The electrical resistance of all samples was found to be reduced under compression loads, but its resistance was regained again when the load was removed. This resistance change during the experiment might possibly be due to the opening and closing of voids, defects, and pores in the samples. Chen and Liu [35] mentioned that the breakdown and rebuilding of the percolation network in a fibre reinforced cementitious system under stress is a dynamic balance process. The former is dominant during the initial loading stage, which is responsible for the formation of new pores and consequently decreases the electrical resistivity with increasing stress. The counterbalance of these two occurs when the stress reaches its critical value, which indicates that some flaws occur in the cement sample. However, beyond the critical value, the latter becomes predominant and causes the existing network to breakdown, which responds to the resistance effect of the positive pressure coefficient. According to Chen and Liu [35], when the compressive stress reached 57% of the fracture stress, a plateau appeared, where the fractional change in resistance was kept almost the same. Shortly after that, the electrical resistance increased rapidly with increasing stress, which is described as the positive pressure coefficient effect. The piezoresistive response of a cement-based material is described by the change in its electrical resistivity with the external loads applied [2].

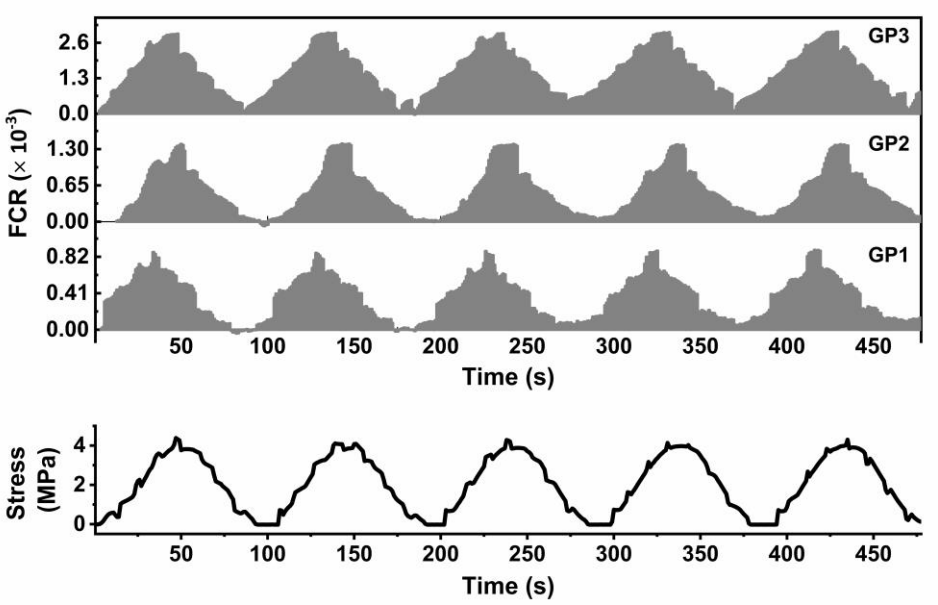

Fig. 8 Electromechanical test results revealing the GP piezoresistive response under external loads

The factorial change in the electrical resistivity (FCR) value is calculated according to Equation 1, where ρ_i and ρ_f are the initial and final electrical resistivities of the porous material [36]. Table 3 lists the average FCR of the GP mixes of this study determined at the end of 28 days. The average of three replicates were calculated.

$$FCR = (\rho_f - \rho_i) / \rho_i \quad (1)$$

GP1, GP2, and GP3 samples were made with an increasing SF content. At the end of 28 days, these samples exhibited an average FCR of about 0.014, 0.018, and 0.024, respectively. The FCR of GP3 was calculated to be 1.7 times higher than that of GP1 when the amount of SF included in the GP mixes increased to 35%. The GP mixes designed with higher amounts of SF was found to display an improved self-sensing potential. The micropores in a cement-based material play a role in the mechanism of contact conduction for piezoresistivity. The concrete piezoresistivity, which results from the variation in the resistance to contact between functional fillers and between the fillers and the cement matrix under compressive loading, is due to the conduction effect of contact and tunnelling [37]. The exploitation of the piezoresistive effect of a GP mix can control the damage of a structural component by recording the variation of its electrical resistance, thus avoiding the application of embedded sensors, which are usually expensive and have limited durability.

3.4. Analysis of pore solution

The average pH of the pore solution extracted from GP1, GP2, and GP3 at the end of 28 days was determined to be 12.32, 11.84, and 11.07. The alkalinity of the pore solution reduced with increasing SF content in the GP mixes. Water effectively dissolved the KOH pellets, thus improving the alkalinity of the pore solution in the GP mix, but its amount should still be limited to avoid a weak self-sensing character. The pore solution in the GP mix was mainly occupied with K^+ and Si^{4+} ions because KOH and SF were used along with MK in the geopolymerization process. Traces of Al^{3+} ions, as shown in Table 3 were also found in such a solution. The concentration of these ions in the pore solution decreased with time, which might be due to the late consumption of such ions by the unreacted aluminosilicate material. The GP3 pore solution was found to have the highest amounts of K^+, Si^{4+}, and Al^{3+} ions compared to the pore solution extracted from other mixes. The ionic conduction of both geopolymer and cement matrices is associated with the mobility of free ions in the pore solution (i.e., Ca^{2+}, K^+, Na^+, Si^{4+}, Fe^{2+}, Al^{3+} and OH^-) [38]. Free ions that are not bound to the GP matrix can move through the pores to enhance electrical conductivity. Metal cations are bound to the AlO_4^--SiO_4 structure or are present in the cavities of this tetrahedral framework to maintain the electrical charge balance in the GP matrix [11]. The cement matrix is an effective electrical insulator, unless it is wet [39]. The ionic conductivity of the cement matrix is attributed to the mobility of the Ca^{2+} and OH^- ions in the pore solution [40], while the interlaced alkalis within the structure of AlO_4^--SiO_4 greatly influences the ionic conductivity of the GP matrix [41]. Ionic conduction depends on the amount of free water available in the cement matrix, and this binder usually cannot be deployed for sensor applications because the detected conductivity value is too low. However, this ionic conduction of the GP binder is comparatively higher [42].

Table 3 Concentration of Al^{3+}, Si^{4+} and K^+ ions remaining in the pore solution of GP samples

Sample	Aluminium (mg/L)	Silicon (mg/L)	Potassium (mg/L)
GP1	Below detection limits	254	10014
GP2	Below detection limits	385	12572
GP3	3.2	512	11351

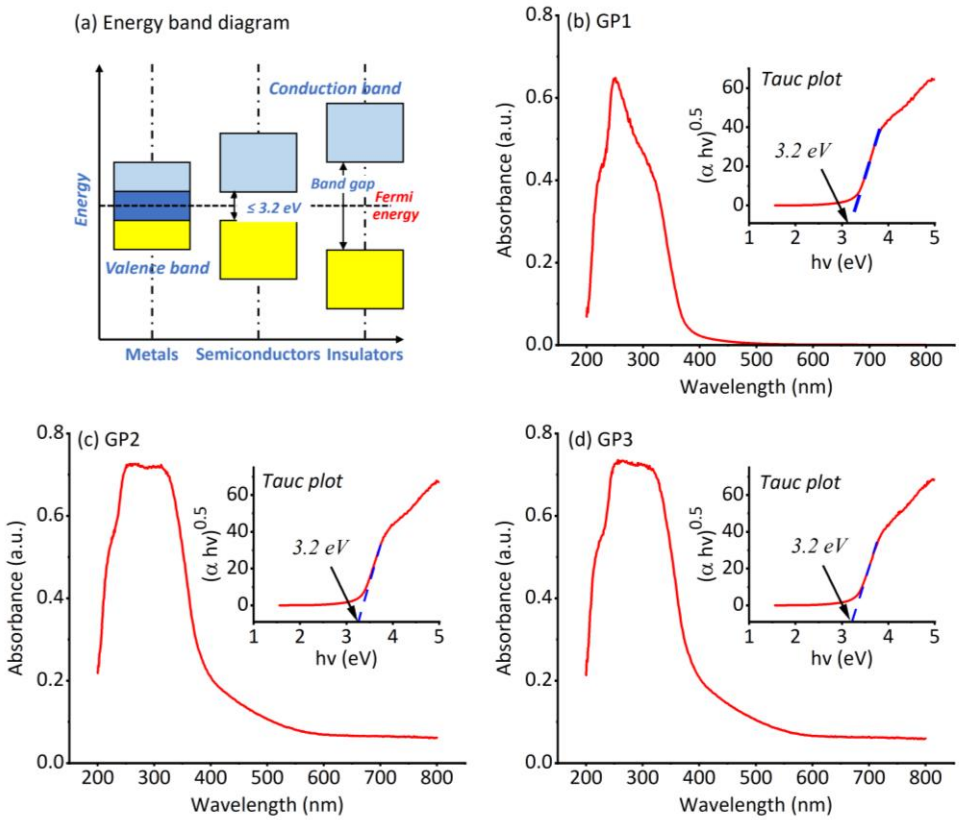

Fig. 9 (a) Energy band diagram for metals, semiconductors, and insulators and (b) results of the UV-Vis spectroscopy analysis (inset images showing their corresponding Tauc plots)

3.5. Microstructural assessment

3.5.1.UV-Vis spectrum

In this study, UV-vis spectroscopy was used to measure the amount of light that a GP binder absorbs. The absorbance of the material is a measure of the amount of light absorbed. Materials are generally classified as metals, semiconductors, and insulators based on band-gap theory. In metals [43], the valence and conduction bands overlap, and thus they are good conductors of heat and electricity. However, in the case of semiconductors and insulators [44], there is a finite gap between the valence and conduction bands. The band gap energy (E) is the energy difference between the valence and conduction bands of the material (in solid state) [45]. Fig. 9a shows the classification of materials using an energy band diagram [45]. The unit of band-gap energy is expressed in electronvolt (eV). The materials are called semiconductors when the photon energy is less than or equal to 3.2 eV. If this energy is greater than 3.2 eV, then the material is called an insulator. When sufficient energy is provided to semiconductor materials, the electrons from the valence band overcome the band gap energy and move into the conduction band. Thus, the electrical conductivity of the semiconductor lies in the vicinity of that of metals and insulators [44]. Tauc [46] and Boudad et al. [47] estimated the optical band gap energy (Eg) of a porous material based on its absorbance information. A Tauc plot is one method to determine the optical band gap in semiconductors. The square root of the product of the absorption coefficient and the photon energy ($(\alpha h\nu)^{0.5}$) is plotted versus the photon energy (hv). The curve should have a straight-line section. When extended to the x-axis, the x-intercept of this line gives the optical band gap. Equation 2 proposed by Tauc [46] relates the optical absorbance coefficient (α) with the energy band gap, where A is a proportionality constant depending on the material, and n is a constant that depends on the nature of the transition (2 for an indirect allowed transition and 0.5 for a direct allowed transition).

$$\alpha h_v = A(h_V - E_g)^n \quad (2)$$

Fig. 9 also presented the absorbance spectra of GP1, GP2, and GP3 obtained at the end of 28 days. The samples are found to represent an indirect optical band gap, and the extrapolation of the $(\alpha h\nu)^{0.5}$ versus hv (inset images in Fig. 9) to the zero value of $(\alpha h\nu)^{0.5}$ gives an indirect optical band gap energy of about 3.2 eV for all GP samples, which confirms the semiconductor behaviour of such samples.

3.5.2.FTIR, XRD, and SEM results

Fig. 10 and Fig. 11 show the FTIR and XRD results. The main mid-IR bands at wavelengths 3390, 1640, 974, and 571 cm^{-1} were attributed to the O-H, H-O-H, and Si(Al)-O and Al-O stretching and bending modes. The intensity of such bands was found to be almost the same in both samples. The availability of these functional groups in a GP sample indicated the formation of a 3D network with SiO_4 and AlO_4 tetrahedrons,

cross-linked by oxygen bridging. Alkalis and metal cations (i.e., K^+, Na^+, Ca^{2+}, and H_3O^+) fill the cavities in these networks, balancing the negative charge of Al^{3+} ions. At a low SiO_2/Al_2O_3 molar ratio, the silicate and aluminate species in the GP matrix were linked to form a zeolite-like structure [48]. In this study, the major XRD peaks at 14.9°, 28.1°, and 48.1° 2θ (and 46-1045, 84-1285, and 1-562 powder diffraction file numbers given by the international center for diffraction data) confirmed the availability of quartz (SiO_2) and also traces of kaolinite ($Al_2Si_2O_5(OH)_4$) and anatase (TiO_2) in the GP samples. Koleżyński et al. [49] found that the MK-based GP mix underwent crystallisation rather than polymerisation when the alkaline solution used did not contain sodium silicate. Fig. 12 shows the microstructure of the GP samples at the end of 28 days obtained by SEM investigation. They were found to be composed of unreacted metakaolin (i.e., precursor) and alkali aluminosilicate gels (i.e., GP reaction products). GP1 was found to have more angular MK particles in its matrix compared to GP3. Multiple EDS points were collected on a wide area of GP surfaces to quantify the elemental composition of the formed reaction products. The atomic ratio of Si/Al (in X-axis) versus K/Al (in Y-axis) obtained from such products was plotted to validate the GP gel structure. If the Si/Al ratio is low, then the GP reaction products are capable of substituting Al^{3+} ions into silicate tetrahedral networks to generate a poly(sialate) structure [48]. Fig. 13 shows the 2D scatter plots that were drawn using these atomic ratios calculated from the EDS point analyses. The Si/Al molar ratio of the GP1 reaction products was found to be lower than that of other samples, which is because the GP1 matrix was activated with the KOH solution that contained the lowest SF content. Juengsuwattananon et al. [48] determined the structure of the GP reaction products with the EDS information and evaluated the rate of their reaction in the stages of dissolution and polycondensation. In this study, the Si/Al ratio of MK calculated with the XRF results was almost 1.2. The GP samples were found to have a Si/Al ratio between 1.2-1.9, indicating that the gel structure might be poly(sialate) and poly(sialate-siloxo).

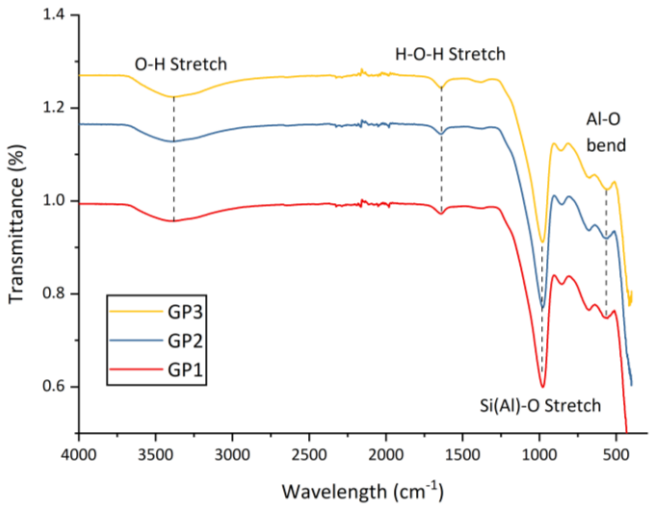

Fig. 10 FTIR results of the GP samples at the end of 28 days

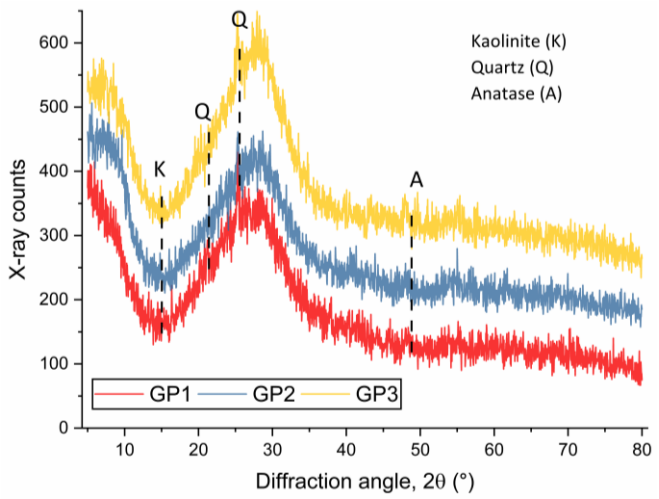

Fig. 11 XRD results of the GP samples at the end of 28 days

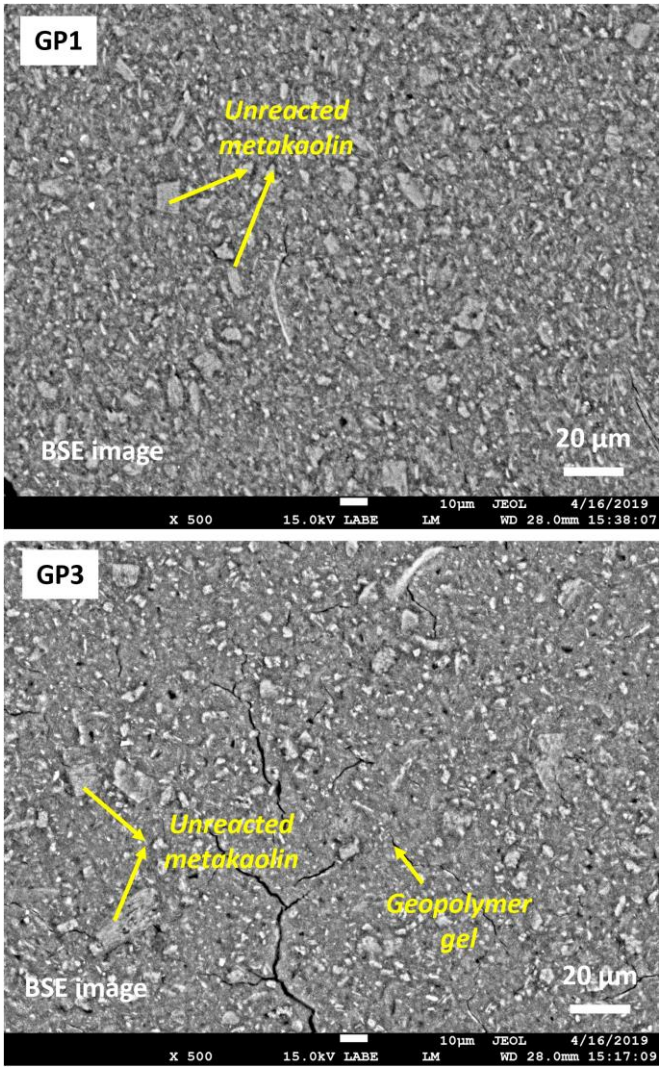

Fig. 12 SEM images revealing the microstructure of the different GP samples

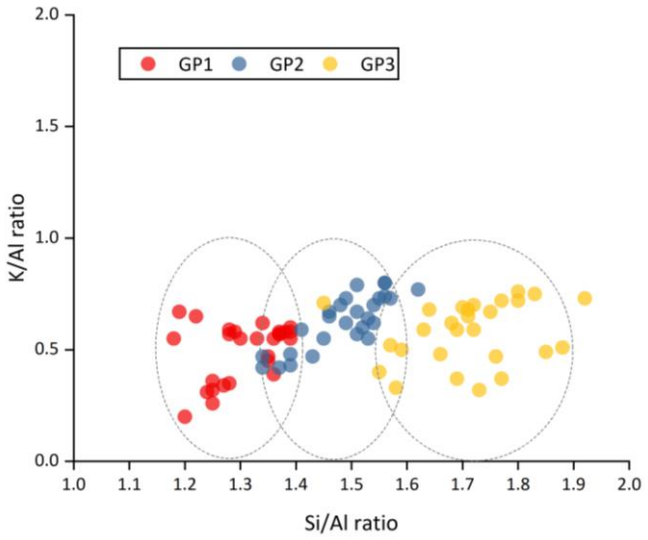

Fig. 13 EDS scatter plots of the different GP samples

4. CONCLUSIONS

The piezoresistivity effects of GP mixes that were made with SF-derived alkaline activators of different composition were investigated. The key findings are listed below.

- Fresh GP samples exhibited a delayed setting when the SF content was maximum, suggesting that the SF content should be optimum while GP mixes are designed to avoid setting issues.
- No major change in the strength gain of the GP binder after 3 days, indicating that this low carbon material attained the maximum compressive strength within a few days of casting. Adding more SF improved the compressive strength of the GP mixes.
- The GP mix designed with an alkaline solution-to-precursor ratio of 2.5 by weight was found to exhibit the highest FCR among the mixes. The chemical ratios K_2O/Al_2O_3, SiO_2/Al_2O_3, and H_2O/K_2O of this alkaline solution were calculated as 1.2, 4, and 15 by weight. The GP mix designed with higher amounts of SF was found to display improved self-sensing potential.
- The pore solution in the GP mix was mainly occupied with K^+ and Si^{4+} ions because KOH and SF were used along with MK in the polymerization process. Traces of Al^{3+} ions were also found in such a solution. The pore solution extracted from the GP mix made with the higher SF content was found to have the highest amounts of K^+, Si^{4+}, and Al^{3+} ions than the pore solution extracted from other mixes.
- The XRD pattern confirms the major availability of quartz and traces of kaolinite and anatase in all GP samples. These experimental findings suggest that the addition of more SF to the KOH solution improved the piezoresistivity of the GP binder, which has shown potential to monitor concrete structures under cyclic compression. Future research could involve examination of its self-sensing performance under bending and as embedded sensors in larger concrete structures. It is believed that a geopolymer concrete with ultrahigh sensitivity can be used as an ideal self-sensing structural material.

REFERENCES

[1] Y. Zhang, J. Wang, J. Wang, and X. Qian, "Preparation, mechanics and self-sensing performance of sprayed reactive powder concrete," *Science Reports*, vol. 12, no. 1, p. 7787, 2022/05/12 2022, doi: https://doi.org/10.1038/s41598-022-11836-y.

[2] B. Han, S. Ding, and X. Yu, "Intrinsic self-sensing concrete and structures: A review," *Measurement*, vol. 59, pp. 110-128, 2015/01/01/ 2015, doi: https://doi.org/10.1016/j.measurement.2014.09.048.

[3] S. Wen and D. D. L. Chung, "Cement-based materials for stress sensing by dielectric measurement," *Cement and Concrete Research*, vol. 32, no. 9, pp. 1429-1433, 2002/09/01/ 2002, doi: https://doi.org/10.1016/S0008-8846(02)00789-5.

[4] Y. Guo *et al.*, "Self-sensing performance of cement-based sensor with carbon black and polypropylene fibre subjected to different loading conditions," *Journal of Building Engineering*, vol. 59, p. 105003, 2022/11/01/ 2022, doi: https://doi.org/10.1016/j.jobe.2022.105003.

[5] Z. Tian, Y. Li, J. Zheng, and S. Wang, "A state-of-the-art on self-sensing concrete: Materials, fabrication and properties," *Composites Part B: Engineering*, vol. 177, p. 107437, 2019/11/15/ 2019, doi: https://doi.org/10.1016/j.compositesb.2019.107437.

[6] T. W. Ebbesen, H. J. Lezec, H. Hiura, J. W. Bennett, H. F. Ghaemi, and T. Thio, "Electrical conductivity of individual CNTs," *Nature*, vol. 382, no. 6586, pp. 54-56, 1996/07/01 1996, doi: https://doi.org/10.1038/382054a0.

[7] M. Jung, J. Park, S.-g. Hong, and J. Moon, "Electrically cured UHPC embedded with CNTs for field casting and crack sensing," *Materials & Design*, vol. 196, p. 109127, 2020/11/01/ 2020, doi: https://doi.org/10.1016/j.matdes.2020.109127.

[8] J. Davidovits, "Properties of geopolymer cements," in *First international conference on alkaline cements and concretes*, 1994, vol. 1: Kiev State Technical Laboratory, pp. 131-149.

[9] J. McAlorum, M. Perry, C. Vlachakis, L. Biondi, and B. Lavoie, "Robotic spray coating of self-sensing metakaolin geopolymer for concrete monitoring," *Automation in Construction*, vol. 121, p. 103415, 2021/01/01/ 2021, doi: https://doi.org/10.1016/j.autcon.2020.103415.

[10] P. Duxson, "Geopolymer precursor design," in *Geopolymers*, J. L. Provis and J. S. J. van Deventer Eds.: Woodhead Publishing, 2009, pp. 37-49.

[11] X.-M. Cui, G.-J. Zheng, Y.-C. Han, F. Su, and J. Zhou, "A study on electrical conductivity of chemosynthetic Al_2O_3–$2SiO_2$ geopolymer materials," *Journal of Power Sources*, vol. 184, no. 2, pp. 652-656, 2008/10/01/ 2008, doi: https://doi.org/10.1016/j.jpowsour.2008.03.021.

[12] C. Lamuta, S. Candamano, F. Crea, and L. Pagnotta, "Direct piezoelectric effect in geopolymeric mortars," *Materials & Design*, vol. 107, pp. 57-64, 2016/10/05/ 2016, doi: https://doi.org/10.1016/j.matdes.2016.05.108.

[13] M. Saafi *et al.*, "Graphene/fly ash geopolymeric composites as self-sensing structural materials," *Smart Materials and Structures*, vol. 23, no. 6, p. 065006, 2014, doi: https://doi.org/10.1088/0964-1726/23/6/065006.
[14] M. Saafi *et al.*, "Multifunctional properties of carbon nanotube/fly ash geopolymeric nanocomposites," *Construction and Building Materials*, vol. 49, pp. 46-55, 2013/12/01/ 2013, doi: https://doi.org/10.1016/j.conbuildmat.2013.08.007.
[15] S. Bi, M. Liu, J. Shen, X. M. Hu, and L. Zhang, "Ultrahigh self-sensing performance of geopolymer nanocomposites via unique interface engineering," *ACS Applied Materials & Interfaces*, vol. 9, no. 14, pp. 12851-12858, 2017/04/12 2017, doi: https://doi.org/10.1021/acsami.7b00419.
[16] V. Charitha, G. Athira, A. Bahurudeen, and S. Shekhar, "Carbonation of alkali activated binders and comparison with the performance of ordinary Portland cement and blended cement binders," *Journal of Building Engineering*, vol. 53, p. 104513, 2022/08/01/ 2022, doi: https://doi.org/10.1016/j.jobe.2022.104513.
[17] D. Khale and R. Chaudhary, "Mechanism of geopolymerization and factors influencing its development: a review," *Journal of Materials Science*, vol. 42, no. 3, pp. 729-746, 2007/02/01 2007, doi: https://doi.org/10.1007/s10853-006-0401-4.
[18] J. Cai, J. Tan, and X. Li, "Thermoelectric behaviors of fly ash and metakaolin based geopolymer," *Construction and Building Materials*, vol. 237, p. 117757, 2020/03/20/ 2020, doi: https://doi.org/10.1016/j.conbuildmat.2019.117757.
[19] R. B. Polder, "Test methods for on site measurement of resistivity of concrete — a RILEM TC-154 technical recommendation," *Construction and Building Materials*, vol. 15, no. 2, pp. 125-131, 2001/03/01/ 2001, doi: https://doi.org/10.1016/S0950-0618(00)00061-1.
[20] P. Duxson, J. L. Provis, G. C. Lukey, S. W. Mallicoat, W. M. Kriven, and J. S. J. van Deventer, "Understanding the relationship between geopolymer composition, microstructure and mechanical properties," *Colloids and Surfaces A: Physicochemical and Engineering Aspects*, vol. 269, no. 1, pp. 47-58, 2005/11/01/ 2005, doi: https://doi.org/10.1016/j.colsurfa.2005.06.060.
[21] P. He *et al.*, "Effects of Si/Al ratio on the structure and properties of metakaolin based geopolymer," *Ceramics International*, vol. 42, no. 13, pp. 14416-14422, 2016/10/01/ 2016, doi: https://doi.org/10.1016/j.ceramint.2016.06.033.
[22] M. Sellami, M. Barre, and M. Toumi, "Synthesis, thermal properties and electrical conductivity of phosphoric acid-based geopolymer with metakaolin," *Applied Clay Science*, vol. 180, p. 105192, 2019/11/01/ 2019, doi: https://doi.org/10.1016/j.clay.2019.105192.
[23] *Standard test method for measurement of heat of hydration of hydraulic cementitious materials using isothermal conduction calorimetry*, ASTM C1702, Pennsylvania, United States, 2017.
[24] *Standard test method for compressive strength of hydraulic cement mortars*, ASTM C109, Pennsylvania, United States, 2016.
[25] H. Ma, D. Hou, and Z. Li, "Two-scale modeling of transport properties of cement paste: Formation factor, electrical conductivity and chloride diffusivity," *Computational Materials Science*, vol. 110, pp. 270-280, 2015/12/01/ 2015, doi: https://doi.org/10.1016/j.commatsci.2015.08.048.
[26] N. Ukrainczyk, M. Muthu, O. Vogt, and E. Koenders, "Geopolymer, calcium aluminate, and Portland cement-based mortars: comparing degradation using acetic acid," *Materials*, vol. 12, no. 19, p. 3115, 2019, doi: https://doi.org/10.3390/ma12193115.
[27] G. Liang, W. Yao, and A. She, "New insights into the early-age reaction kinetics of metakaolin geopolymer by 1H low-field NMR and isothermal calorimetry," *Cement and Concrete Composites*, vol. 137, p. 104932, 2023/03/01/ 2023, doi: https://doi.org/10.1016/j.cemconcomp.2023.104932.
[28] Z. Li, S. Zhang, Y. Zuo, W. Chen, and G. Ye, "Chemical deformation of metakaolin based geopolymer," *Cement and Concrete Research*, vol. 120, pp. 108-118, 2019/06/01/ 2019, doi: https://doi.org/10.1016/j.cemconres.2019.03.017.
[29] M. Schmücker and K. J. D. MacKenzie, "Microstructure of sodium polysialate siloxo geopolymer," *Ceramics International*, vol. 31, no. 3, pp. 433-437, 2005/01/01/ 2005, doi: https://doi.org/10.1016/j.ceramint.2004.06.006.
[30] P. D. Silva, K. Sagoe-Crenstil, and V. Sirivivatnanon, "Kinetics of geopolymerization: Role of Al2O3 and SiO2," *Cement and Concrete Research*, vol. 37, no. 4, pp. 512-518, 2007/04/01/ 2007, doi: https://doi.org/10.1016/j.cemconres.2007.01.003.
[31] P. De Silva and K. Sagoe-Crenstil, "Medium-term phase stability of Na_2O–Al_2O_3–SiO_2–H_2O geopolymer systems," *Cement and Concrete Research*, vol. 38, no. 6, pp. 870-876, 2008/06/01/ 2008, doi: https://doi.org/10.1016/j.cemconres.2007.10.003.
[32] F. Zhang, L. Zhang, M. Liu, C. Mu, Y. N. Liang, and X. Hu, "Role of alkali cation in compressive strength of metakaolin based geopolymers," *Ceramics International*, vol. 43, no. 4, pp. 3811-3817, 2017/03/01/ 2017, doi: https://doi.org/10.1016/j.ceramint.2016.12.034.
[33] S. A. Bernal, E. D. Rodríguez, R. Mejia de Gutiérrez, J. L. Provis, and S. Delvasto, "Activation of Metakaolin/Slag Blends Using Alkaline Solutions Based on Chemically Modified Silica Fume and Rice Husk Ash," *Waste and Biomass Valorization*, vol. 3, no. 1, pp. 99-108, 2012/03/01 2012, doi: https://doi.org/10.1007/s12649-011-9093-3.
[34] N. Billong, J. Oti, and J. Kinuthia, "Using silica fume based activator in sustainable geopolymer binder for building application," *Construction and Building Materials*, vol. 275, p. 122177, 2021/03/15/ 2021, doi: https://doi.org/10.1016/j.conbuildmat.2020.122177.
[35] B. Chen and J. Liu, "Damage in carbon fiber-reinforced concrete, monitored by both electrical

resistance measurement and acoustic emission analysis," *Construction and Building Materials*, vol. 22, no. 11, pp. 2196-2201, 2008/11/01/ 2008, doi: https://doi.org/10.1016/j.conbuildmat.2007.08.004.

[36] C. Mizerová, I. Kusák, L. Topolář, P. Schmid, and P. Rovnaník, "Self-sensing properties of fly ash geopolymer doped with carbon black under compression," *Materials*, vol. 14, no. 16, p. 4350, 2021, doi: https://doi.org/10.3390/ma14164350.

[37] J. Ou and B. Han, "Piezoresistive cement-based strain sensors and self-sensing concrete components," *Journal of Intelligent Material Systems and Structures*, vol. 20, no. 3, pp. 329-336, 2009, doi: https://doi.org/10.1177/1045389x08094190.

[38] I. L. H. Hansson and C. M. Hansson, "Ion-conduction in cement-based materials," *Cement and Concrete Research*, vol. 15, no. 2, pp. 201-212, 1985/03/01/ 1985, doi: https://doi.org/10.1016/0008-8846(85)90031-6.

[39] X. Wang, A. Al-Tabbaa, and S. K. Haigh, "Measurement techniques for self-sensing cementitious composites under flexure," *Cement and Concrete Composites*, vol. 142, p. 105215, 2023/09/01/ 2023, doi: https://doi.org/10.1016/j.cemconcomp.2023.105215.

[40] S. Rengaraju, R. G. Pillai, R. Gettu, and L. Neelakantan, "Effect of test methods on corrosion phenomena of steel in highly resistive concrete systems and data interpretations," *Corrosion*, vol. 77, no. 4, pp. 445-459, 2021, doi: https://doi.org/10.5006/3705.

[41] J. L. Provis, "Geopolymers and other alkali activated materials: why, how, and what?," *Materials and Structures*, vol. 47, no. 1, pp. 11-25, 2014/01/01 2014, doi: https://doi.org/10.1617/s11527-013-0211-5.

[42] P. Duxson, A. Fernández-Jiménez, J. L. Provis, G. C. Lukey, A. Palomo, and J. S. J. van Deventer, "Geopolymer technology: the current state of the art," *Journal of Materials Science*, vol. 42, no. 9, pp. 2917-2933, 2007/05/01 2007, doi: https://doi.org/10.1007/s10853-006-0637-z.

[43] J. Li and D. Chu, "4 - Energy band engineering of metal oxide for enhanced visible light absorption," in *Multifunctional photocatalytic materials for energy*, Z. Lin, M. Ye, and M. Wang Eds.: Woodhead Publishing, 2018, pp. 49-78.

[44] C. Richard, "Semiconductor basics," in *Understanding semiconductors: A technical guide for non-technical people*, C. Richard Ed. Berkeley, United States: Apress, 2023, pp. 1-23.

[45] K. Seeger, "Energy Band Structure," in *Semiconductor physics: An introduction*, K. Seeger Ed. Berlin, Germany: Springer, 1997, pp. 10-33.

[46] J. Tauc, "Optical properties and electronic structure of amorphous Ge and Si," *Materials Research Bulletin*, vol. 3, no. 1, pp. 37-46, 1968/01/01/ 1968, doi: https://doi.org/10.1016/0025-5408(68)90023-8.

[47] L. Boudad, M. Taibi, A. Belayachi, and M. Abd-Lefdil, "Dielectric relaxation, electrical conductivity and optical studies of solid-state synthesized EuCrO3," *Journal of Materials Science: Materials in Electronics*, vol. 31, no. 1, pp. 354-360, 2020/01/01 2020, doi: https://doi.org/10.1007/s10854-019-02533-0.

[48] K. Juengsuwattananon, F. Winnefeld, P. Chindaprasirt, and K. Pimraksa, "Correlation between initial SiO_2/Al_2O_3, Na_2O/Al_2O_3, Na_2O/SiO_2 and H_2O/Na_2O ratios on phase and microstructure of reaction products of metakaolin-rice husk ash geopolymer," *Construction and Building Materials*, vol. 226, pp. 406-417, 2019/11/30/ 2019, doi: https://doi.org/10.1016/j.conbuildmat.2019.07.146.

[49] A. Koleżyński, M. Król, and M. Żychowicz, "The structure of geopolymers – Theoretical studies," *Journal of Molecular Structure*, vol. 1163, pp. 465-471, 2018/07/05/ 2018, doi: https://doi.org/10.1016/j.molstruc.2018.03.033.